

# Phase-change annealing effects on electrical and optical properties of tin oxide thin films

V. S. SENTHIL SRINIVASAN, M. K. PATRA<sup>a</sup>, V. S. CHOUDHARY<sup>a</sup>, M. MATHEW<sup>a</sup>, A. PANDYA<sup>a\*</sup>

*Center of Excellence in Nanoelectronics, Indian Institute of Technology Bombay, Powai, Mumbai-400076, India.*

*<sup>a</sup>Defence Laboratory, Defence R&D Organisation, Ratanada Palace, Jodhpur, Rajasthan-342011, India.*

The change from tetragonal to orthorhombic phase due to annealing also changes the electrical and optical properties of tin oxide thin films. X-ray diffraction and Atomic force microscopy studies reveal the changes in the phase and grain merger with annealing of as-grown tin oxide thin films. Optical bandgap increase with annealing confirms the improvement in the quality of film transparency. Electrical conductivity also shows an increasing trend with annealing. Parameters such as activation energy, optical bandgap, average roughness, and extinction coefficient have been determined and interpreted with respect to annealing.

(Received March 9, 2010; accepted July 14, 2010)

*Keywords:* Electron-beam evaporation, Thin films, Annealing, Tin oxide, Orthorhombic, Phase change, Atomic Force Microscopy, Activation energy.

## 1. Introduction

There has been great interest in the gas-sensing properties of tin oxide, because it is n-type and is very sensitive to the surroundings. Tin oxide is extensively used as an optically transparent, electrically conducting, and high-bandgap material for optoelectronic applications, solar cells, and liquid crystal displays, etc.<sup>1-3</sup> Tin oxide thin films have a band gap of 3.6 eV,<sup>4</sup> useful in various applications for low electrical resistance (resulting in high conductivity) with high transparency in the visible region. Doped and undoped tin oxide thin films were prepared by spray pyrolysis,<sup>4,5</sup> magnetron sputtering,<sup>6</sup> and reactive electron beam evaporation.<sup>7</sup> Among these fabrication methods, the electron-beam evaporation technique has received much attention because of its very low deposition rate, good adhesion, and ability to produce thin films with larger area. Tin oxide thin films are most frequently produced in SnO and/or SnO<sub>2</sub> phases. The SnO<sub>2</sub> phase is by far the most studied because of its considerable technological importance and stability. Moreno *et al.* have analyzed and reported about the deviation in stoichiometry due to metal vacancies of the tin monoxide phase. The mechanism of the transformation from SnO phase to SnO<sub>2</sub> phase is poorly understood.<sup>8</sup> At room temperature the tetragonal phase of SnO is stable.<sup>9, 10</sup> Under normal conditions, SnO<sub>2</sub> exists in the most important crystalline phase known as cassiterite, which has a rutile tetragonal crystal structure. Another form of SnO<sub>2</sub> with an orthorhombic structure is known to be stable only at high pressures and temperatures. However, the orthorhombic phase of SnO<sub>2</sub> has been produced by oxidizing epitaxial SnO thin film by Kraševc *et al.*<sup>11</sup> Both phases are known to undergo phase transformations to orthorhombic variants at high pressures.<sup>12, 13</sup> In the present study, we synthesized the stable tin oxide thin film at 250°C by the electron-

beam evaporation technique. Further annealing of these films is carried out at different temperatures and we studied their morphology, and structural, electrical, and optical properties. In our experiments, we produced orthorhombic tin dioxide by annealing the tetragonal tin monoxide at 600°C in air atmosphere.

## 2. Experimental

Tin oxide thin films were deposited on soda-lime glass using SnO<sub>2</sub> (Sigma-Aldrich, 99.99% purity) powder as the starting material. The evaporation and deposition was performed in a high-vacuum chamber by bombarding the SnO<sub>2</sub> using a bent-beam electron gun. Prior to loading the soda-lime glass substrates into the chamber, the substrates were cleaned thoroughly in NaOH detergent and then rinsed in deionized water. Finally, the substrates were ultrasonically cleaned in ethanol. To grow the thin films with good adhesion, the substrate temperature was set at 250°C. The chamber pressure was pumped to about 10<sup>-6</sup> mbar before evaporation and to about 2x10<sup>-5</sup> mbar during evaporation. The rate of deposition of thin films was controlled by a quartz-crystal monitor. In this way, the tin oxide thin films were deposited on glass substrates at a deposition rate of 1.5 Å/s and to a thickness of 500 nm.

The as-grown films were annealed at atmospheric pressure in the high-temperature furnace for one hour at 400°, 500°, and 600 °C for different samples, namely, Ann 400°C, Ann 500°C and Ann 600°C respectively. After this process, the furnace was cooled naturally to room temperature. The crystal structure of the as-grown and annealed samples was characterized by X-ray diffraction (XRD)<sup>[14]</sup> using PANALYTICAL X'Pert PRO. The X-ray wavelength ( $\lambda$ ) used in our experiment is 1.936 Å by Fe source. The surface morphology of the as-grown and

annealed thin films was examined by using a NTMDT Solver Pro-M Scanning Probe Microscope operating in semi-contact mode. The optical studies of the as-grown and annealed films were made by using a Perkin-Elmer Lambda 900 double beam UV-VIS-NIR Spectro photometer. Electrical contacts of the tin oxide thin films were formed by fine copper leads using silver paste. All measurements were done with a Keithley Electrometer 6517A.

### 3. Results and discussion

Fig. 1 depicts the XRD pattern of as-grown and annealed tin oxide thin films. From the figure, as-grown film shows diffraction peaks corresponding to (001), (101), (002), (112), and (211) planes of the tetragonal SnO structure (JCPDS No. 06-0395). The sample annealed at 400°C shows a similar XRD pattern and further annealing at 500°C, the diffraction peaks corresponding to (110), (006), and (115) related to the SnO<sub>2</sub> orthorhombic phase are observed. As can be seen from Fig. 1(c), the peaks corresponding to ((101) + (113)), the polycrystalline phases are overlapping peaks, which could be attributed to a mixture of tetragonal SnO with orthorhombic SnO<sub>2</sub>. This result indicates that the phase transformation of SnO tetragonal to SnO<sub>2</sub> orthorhombic occurs after annealing at 400°C. The presence of low-intensity peaks points out that besides the predominating polycrystalline-like phase, the grown film contains some amorphous-like (poorer polycrystalline) phases, as well. Unfortunately, because of the low intensities, the attempt to split the overlapping peak and obtain more detailed information about the film was not successful. Further, on annealing of these films at 600°C, we observed the diffraction peaks corresponding to the SnO<sub>2</sub> orthorhombic phase (JCPDS No. 78-1063) exhibit a strong orientation along the (113) direction, with the development of a new peak (112). Thus, the present

analysis on annealing of tin monoxide in the tetragonal phase at 600°C shows the conversion into the SnO<sub>2</sub> orthorhombic phase. Oxidizing the epitaxial tin monoxide films at ambient phase into the orthorhombic phase may be ascribed to a misfit strain originating at the substrate interface.<sup>15</sup> However, the orthorhombic phase was also observed in a wide variety of powder samples, which are unconstrained by substrate interactions, produced by wet-chemical methods. Formation of the orthorhombic SnO<sub>2</sub> phase by oxidizing the tetragonal SnO at ambient pressure in this work may be attributable to the lower nucleation barrier from a steric effect of tin and oxygen atoms<sup>16</sup> for the dominated peak in the XRD; changes with annealing temperature are listed in Table 1.

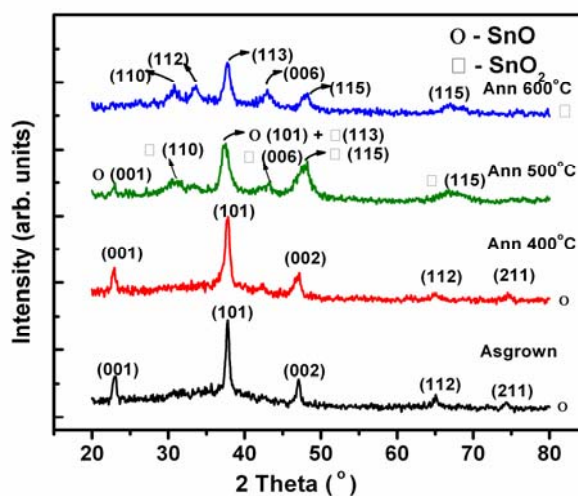


Fig. 1. XRD patterns of tin oxide thin films before and after annealing at 400°, 500° and 600°C for 1 h.

Table 1. Properties of as-grown and annealed tin oxide thin films.

	As-grown	Ann 400°C	Ann 500°C	Ann 600°C
Crystalline Phase*	SnO (T)	SnO (T)	SnO (T) + SnO <sub>2</sub> (O)	SnO <sub>2</sub> (O)
Grain Size (nm)	103	54	92	85
Optical Bandgap E <sub>g</sub> (eV)	2.77	2.80	3.07	3.38
Activation Energy (eV)	1.97	0.64	0.56	0.96
Avg. Roughness (nm)	30.5	14.5	28.7	27
Extinction Coefficient at 450 nm (a.u)	0.31	0.26	0.15	0.04

\* T - Tetragonal  
O - Orthorhombic

AFM images of as-grown and annealed films are shown in Fig. 2. The average grain size and surface roughness of these films are listed in table 1. From the figure, the grains are found to be spherical in shape. From

the table, it is observed that as-grown films have an average grain size of ~103 nm, whereas the average grain size of annealed films were non-linearly changing with the annealing temperatures. The change in grain size with the

annealing temperature can be correlated with the oxidation mechanism of  $\text{SnO}_x$  thin film. On annealing at  $400^\circ\text{C}$ , the figure shows a reduction in grain size as well as surface roughness of the  $\text{SnO}$  thin film. Further increasing the annealing temperature to  $500^\circ\text{C}$ , the average grain size of the film was found to be  $\sim 92$  nm from the AFM images, which is higher than the sample annealed at  $400^\circ\text{C}$ . The average roughness of the film is found to increase in value (Table 1) in this stage as compared to earlier, which may be due to the formation of a mixed phase of  $\text{SnO}$  and  $\text{SnO}_2$ . The higher surface roughness can be associated with the larger grains, because the tendency is for grains to grow by the fusion of adjacent grains when sufficient energy for surface rearrangement is provided by the annealing. Further, on annealing of this film at  $600^\circ\text{C}$ , the  $\text{SnO}_2$  orthorhombic phase shows a slight decrease of roughness values and the grain size is decreased from 92 nm to 84 nm. The above results indicate that the non-linear variation of grain size with annealing temperature occurs due to rapid thermal annealing and cooling process, as well as by crystal phase changes from tetragonal  $\text{SnO}$  to

orthorhombic  $\text{SnO}_2$  at higher annealing temperatures. Table 1 presents the average surface roughness and grain size of as-grown and annealed tin oxide thin films.

Fig. 3 shows the transmittance spectra of as-grown and annealed thin films of tin oxide in the visible wavelength range. From the figure it is observed that all the spectra show an interference pattern; however, the film becomes more transparent as the annealing temperature is raised. As seen in the figure, the transmittance edge shifts toward the lower-wavelength side for annealed films as compared to as-grown films. Also, the transmission edge  $> 650$  nm shifts toward the higher wavelength side. This shows that the films are becoming more transparent and are in a wider wavelength range. Furthermore, as-grown films had a brownish color that disappeared after annealing in ambient conditions. The values of the optical bandgap  $E_g$  for all as-grown and annealed samples were estimated from Mott and Davis' model<sup>17</sup> for the direct allowed transition:  $\alpha(\nu)h\nu = B(h\nu - E_g)^{1/2}$ , where  $\alpha$  is the absorption coefficient,  $E_g$  is the optical bandgap,  $h\nu$  is the energy of the incident photons, and  $B$  is a constant.

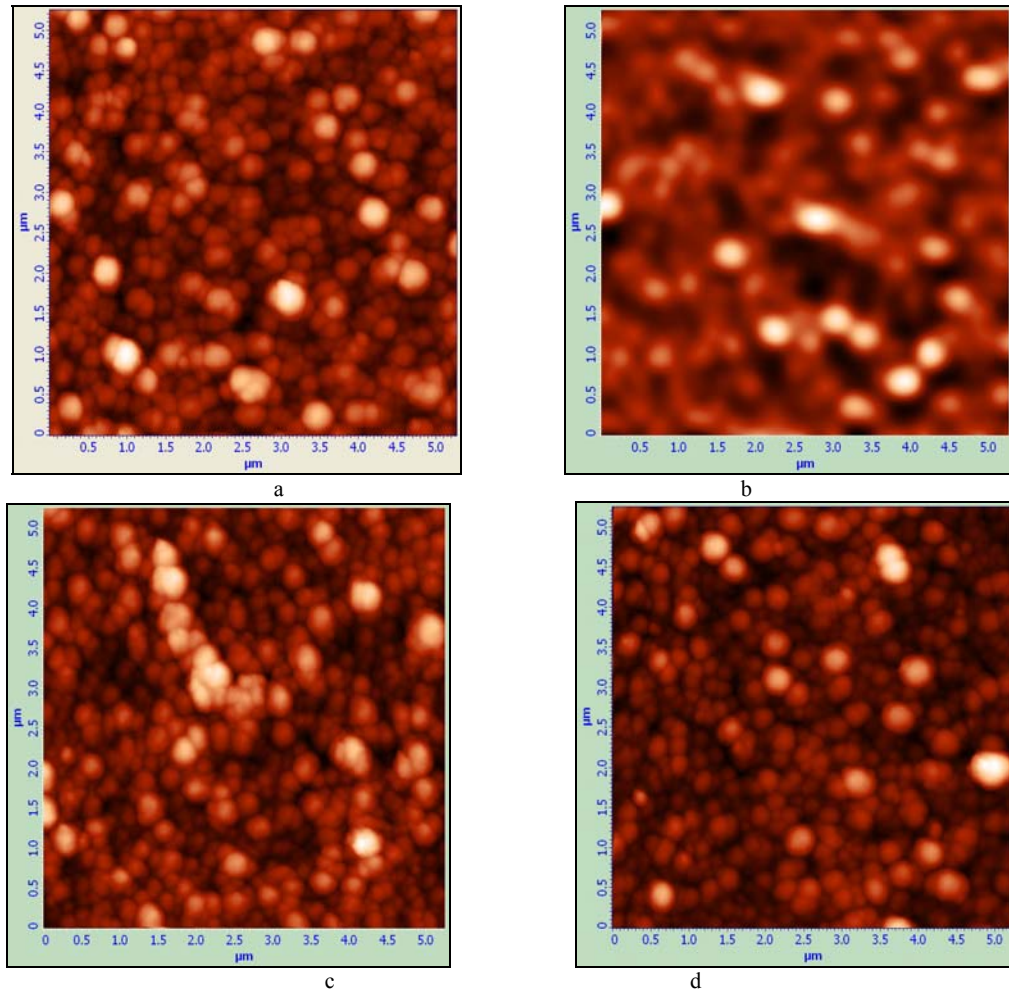


Fig. 2. AFM images of tin oxide thin films before (a) and after annealing at  $400^\circ$  (b),  $500^\circ$  (c) and  $600^\circ\text{C}$  (d) for 1 h, respectively.

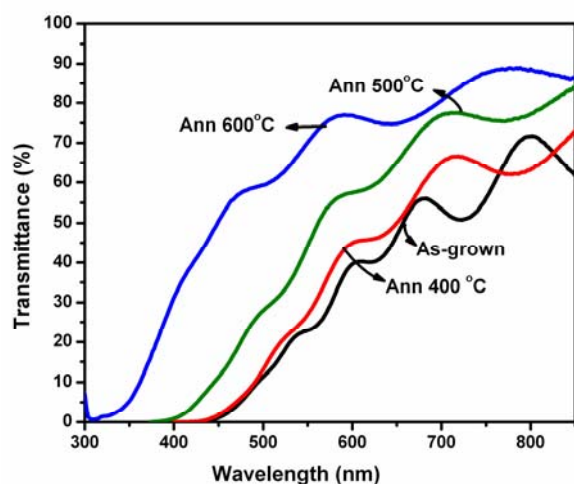


Fig. 3. Optical transmittance spectra of tin oxide thin films before and after annealing at 400°, 500° and 600°C for 1 h.

In Fig. 4, the variation of  $\alpha^2$  versus photon energy is presented for as-grown and annealed films. The straight-line portion of the plot is extrapolated to  $\alpha^2 = 0$  to determine the value of  $E_g$ . As can be seen in Table 1, the derived  $E_g$  values increases with the annealing, which confirms the improvement in tin oxide and formation of tin-dioxide phase. It should be noted that the optical bandgap of tin oxide thin films annealed at 400°C increased from 2.77 to 2.8 eV, with no change in film structure as seen from XRD. This blue shift in bandgap is in view of the reduction in grain size from ~103 to ~54 nm of tetragonal SnO phase. By further annealing at ambient atmosphere, we obtained the bandgap  $E_g = 3.07$  eV for the mixed (SnO + SnO<sub>2</sub>) phase and  $E_g = 3.38$  eV for the SnO<sub>2</sub> orthorhombic thin films. The reported optical bandgap value for orthorhombic SnO<sub>2</sub> thin films falls at ~4.02 eV.<sup>18</sup>

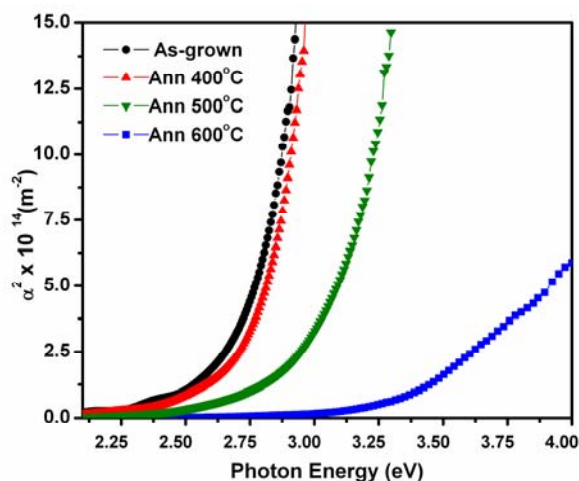


Fig. 4.  $\alpha^2$  vs photon energy of tin oxide thin films before and after annealing at 400°, 500° and 600°C for 1 h.

Fig. 5 shows the variation in extinction coefficient ( $k$ ) with wavelength for as-grown and annealed films. The extinction coefficient  $k$  has been obtained from  $\alpha = 4\pi k/\lambda$ . It is observed that the value of extinction coefficient decreases with the annealing. The decrease of  $k$  value in the shorter-wavelength region after annealing improved the transparency. Such decrease of  $k$  indicates weaker photon absorption by electron transitions in the bandgap where fewer intermediate defect levels could be present after annealing. We also believe that the phase change in tin oxide with annealing affected the changes in the optical parameters.

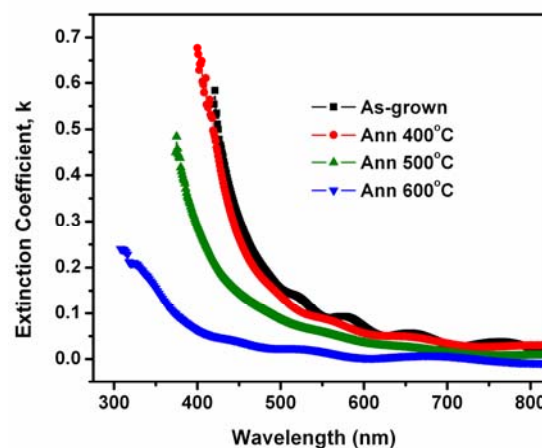


Fig. 5. Extinction Coefficient vs wavelength of tin oxide thin films before and after annealing at 400, 500 and 600 °C for 1 hr.

Fig. 6 depicts the conductivity values with annealing, and it is observed that electrical conductivity increases with the annealing. Subsequently, the transparency also increases with the increase in annealing temperature. This transparent conductivity is related to the existence of shallow donor levels near the conduction band, formed by a large concentration of oxygen vacancies.<sup>19</sup> Figure 7 shows the  $\ln \sigma$  vs  $1/T$  of as-grown and annealed tin oxide films. The DC conductivity of the film is given by  $\sigma = \sigma_0 \exp(-\Delta E_\sigma / K_B T)$ , where  $\sigma$  is the conductivity,  $\sigma_0$  is the pre-exponential factor,  $\Delta E_\sigma$  is activation energy,  $T$  is temperature, and  $K_B$  is the Boltzmann constant. The activation energy of these films is derived from the slope of the  $\ln \sigma$  vs  $1/T$  and presented in Table 1. It is observed that the activation energy of the films is 1.97, 0.64, 0.56, and 0.96 eV for as-grown and 400°, 500°, and 600°C annealed samples, respectively. It is known that for any semiconductor, the activation energy decreases with increasing density of impurities (carriers). It should be noted that in this work the conductivity increased with an increase in annealing temperature, whereas the activation energy shows a decrement at 400°C annealing and further at 500°C annealing. The decrease in activation energy can be attributed to the increase in carrier density and the widening of optical bandgap, as discussed earlier. The

increase in activation energy at 600°C resulted due to the phase transformation from SnO to SnO<sub>2</sub> orthorhombic.

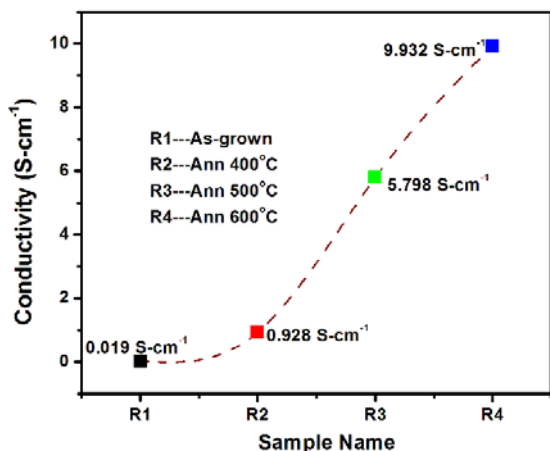


Fig. 6. The dependence of the electrical conductivity of tin oxide thin films on the annealing temperature.

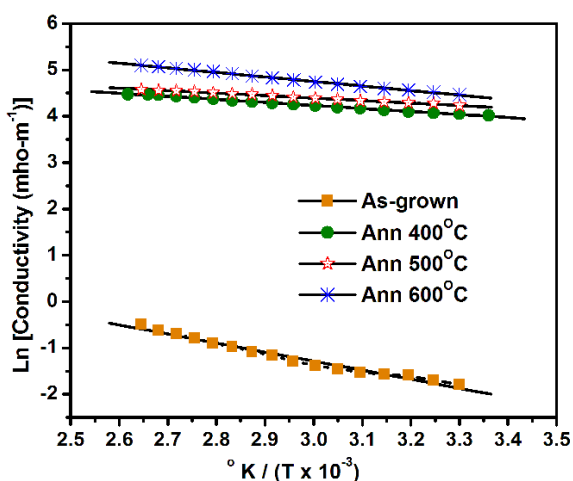


Fig. 7.  $\ln \sigma$  vs  $1/T$  of tin oxide thin films before and after annealing at 400°, 500° and 600°C for 1 h.

#### 4. Summary

Using the electron-beam evaporation method, a stable tetragonal tin monoxide thin film was prepared. From the above results and discussion, we found that annealing of tetragonal tin monoxide thin film at 600°C in atmospheric pressure can change the phase into orthorhombic tin dioxide. This change in the phase can be interpreted as a misfit strain originating at the substrate/thin-film interface. A series of thermal annealing in air atmosphere showed the increase in optical bandgap, transparency and conductivity. The activation energies were 1.97 eV and 0.64 eV for tetragonal SnO and 0.96 eV for orthorhombic

SnO<sub>2</sub> thin films. This work showed that high pressure is not a necessary condition for the formation of the orthorhombic tin dioxide thin films.

#### Acknowledgments

The authors are thankful to Dr. Narendra Kumar, Director, DLJ for support and encouragement to this work. Authors are also thankful to Heads of NRMA and CAM Division for their support to this work.

#### References

- [1] K.L. Chopra, S. Major, D.K. Pandya, *Thin Solid Films* **102**, 1(1983).
- [2] M.W.J. Prins, K.-O. Grosse-Holz, J.F.M. Cillessen, L.F. Feiner, *J. Appl. Phys.* **83** (2), 888 (1998).
- [3] H. Demiryont, K.E. Nietering, R. Surowiec, F.I. Brown, D.R. Plattus, *Appl. Optics* **26**(18), 3803 (1987).
- [4] M. Batzil, U. Diebold, *Prog. Surf. Sci.* **79**, 47 (2005).
- [5] S. Kulaszewicz, *Thin Solid Films* **74**, 211 (1980).
- [6] L. I. Popova et. al., *Thin Solid Films* **186**, 107 (1990).
- [7] K.S. Shamala, L.C.S. Murthy, Narasimha Rao, *Bull. Mater. Sci.* **27**(3), 295 (2004).
- [8] M.S. Moreno, A. Varela, L.C. Otero-Diaz, *Phys. Rev. B*, **56**(9), 5186 (1997).
- [9] R.W.G. Wykcoff, *Crystal Structure* (Wiley, New York, 1965), Vol. 1. p.251.
- [10] W. J. Moore, L. Pauling, *J. Am. Chem. Soc.* **63**, 1392 (1941).
- [11] V. Kraševac, A. Prodan, M. Hudomalj, S. Sulčič, *Phys. Status Solidi A* **87**, 127 (1985).
- [12] D. M. Adams, A. G. Christy, J. Haines, *Phys. Rev. B* **46**, 11358 (1992).
- [13] K. Suito, N. Kawai, Y. Masuda, *Mater. Res. Bull.* **10**, 677 (1975).
- [14] B. D. Cullity, *Elements of X-Ray Diffraction*, 2<sup>nd</sup> Edition, (Addison Wesley Reading, MA, 1978).
- [15] A. Prodon, N. Vene, F. Sevešek, M. Hudomalji, *Thin Solid Films* **147**, 313 (1987).
- [16] F. J. Lamelas, *J. Appl. Phys.* **96**, 6195 (2004).
- [17] N.F. Mott, E.A. Davis, *Electronic Process in Non-Crystalline Materials*, (Clarendon Press, Oxford, UK, 1979).
- [18] Z. Chen, J. K. L. Lai, C.-H. Shek, *Appl. Phys. Lett.* **89**, 231902 (2006).
- [19] Z.M. Jarzebski J.P. Marton, *J. Electrochem.Soc.* **123**(7), 199C (1976).

\*Corresponding author: arunpandya123@gmail.com; sensri@gmail.com